

Article

Kinetics of Zn–C Battery Leaching with Choline Chloride/Urea Natural Deep Eutectic Solvents

Irlanda G. Cruz-Reyes ^{1,2}, Jorge A. Mendoza-Pérez ², Rosario Ruiz-Guerrero ^{3,†}, Dulce Y. Medina-Velázquez ⁴, Luis G. Zepeda-Vallejo ⁴ and Ángel de J. Morales-Ramírez ^{2,5,*} 

¹ Instituto Politécnico Nacional-ESIME, Edificio 2, Av. Luis Enrique Erro S/N, Unidad Profesional Adolfo López Mateos, CDMX 07738, Mexico

² Instituto Politécnico Nacional-ENCB, Departamento de Ingeniería en Sistemas Ambientales, Campus Santo Tomás, Unidad Profesional Lázaro Cárdenas, Prolongación de Carpio y Plan de Ayala s/n, Col. Santo Tomás, CDMX 11340, Mexico

³ Instituto Politécnico Nacional-CIITEC, Calle Cerrada CECATI S/N Col. Santa Catarina Azcapotzalco, CDMX 02250, Mexico

⁴ Departamento de Ingeniería Metalúrgica, Universidad Autónoma Metropolitana, Azcapotzalco, CDMX 02120, Mexico

⁵ Instituto Politécnico Nacional-ESIQIE, Departamento de Ingeniería Metalúrgica, Av. Luis Enrique Erro S/N, Unidad Profesional Adolfo López Mateos, CDMX 07738, Mexico

* Correspondence: amoralesra@ipn.mx; Tel.: +52-55-57296000

† Deceased.



Citation: Cruz-Reyes, I.G.; Mendoza-Pérez, J.A.; Ruiz-Guerrero, R.; Medina-Velázquez, D.Y.; Zepeda-Vallejo, L.G.; Morales-Ramírez, Á.d.J. Kinetics of Zn–C Battery Leaching with Choline Chloride/Urea Natural Deep Eutectic Solvents. *Recycling* **2022**, *7*, 86. <https://doi.org/10.3390/recycling7060086>

Academic Editor: Anna Klemettinen

Received: 10 October 2022

Accepted: 14 November 2022

Published: 18 November 2022

Publisher's Note: MDPI stays neutral with regard to jurisdictional claims in published maps and institutional affiliations.



Copyright: © 2022 by the authors. Licensee MDPI, Basel, Switzerland. This article is an open access article distributed under the terms and conditions of the Creative Commons Attribution (CC BY) license (<https://creativecommons.org/licenses/by/4.0/>).

Abstract: A choline chloride/urea natural deep eutectic solvent (ChCl NADES) was prepared via a green chemistry method and used to leach Zn and Mn oxides from conventional Zn–C scrap batteries. FTIR and ¹H NMR spectroscopy were used to characterize the NADES. The leaching kinetics of the Zn and Mn oxides was monitored at isothermal conditions (80, 100, 125, and 150 °C) and at two solid/NADES ratios: 3.3 and 10 g dm⁻³. It was possible to dissolve Zn and Mn oxides under all of tested conditions, reaching more than a 95% recovery for both metals at 150 °C after 90 min, whereas, at 25 °C, it was possible to leach up to 90% of the Zn and 30% of the Mn after 4320 min (72 h). Furthermore, the leaching kinetics was controlled by the boundary layer, coincident with a shrinking core model. According to the Arrhenius plot, the activation energy for Zn ranges from 49.13 to 52.21 kJ mol⁻¹, and that for Mn ranges from 46.97 to 66.77 kJ mol⁻¹.

Keywords: natural deep eutectic solvents; battery recycling; Zn leaching; Mn leaching; shrinking core model kinetics

1. Introduction

The deep eutectic solvents (DESs) are considered to be a new, alternative family of solvents applied in green chemistry that, used in conjunction with natural compounds, form natural deep eutectic solvents (NADESs). DESs can be defined as mixtures of two or more solid compounds containing hydrogen-bond donors (HBD) and hydrogen-bond acceptors (HBA) that form liquids with melting points much lower than those of the individual components due to self-association [1–3]. In such a way, the newly formed eutectic phase presents a melting point that is generally lower than 100 °C, in comparison to that of each component [4].

Experimental and theoretical studies have shown that the highest fraction of hydrogen bonds in DES preparation is intramolecular and occurs between the HBD and the halide anion. The anion-HBD hydrogen bond network is the basis of the fundamental properties of DES; the structure/conformation and the extent of the HBD interaction, which are the factors that together originate different hydrogen bonding networks in DES, thus determining their structure [5]. The ChCl/urea DES shows a well-established hydrogen bond network between the salt and the HBD, leading to a higher melting point [6].

M.B. Singh et al. mention that the properties of hydrogen bonds cause DESs to have efficient dissolution properties in soluble and insoluble compounds, such as metal oxides in choline chloride: urea DES [7]. Abbott et al. prepared three DESs from ChCl to dissolve metal oxides, such as CuO and ZnO, finding that the hydrogen bonds formed between urea and ChCl achieve an open structure that facilitates transfer-proton transfer and the dissolution of metal, as well as complexation with the metal [3,8,9]. In addition to studying the interactions that exist within the preparation, it is essential to know other advantages that make these DESs into technological materials: these solvents must be friendly to the environment, non-toxic, generally biodegradable and recyclable, non-volatile, non-flammable, and often synthesizable using economical components [2,10,11].

Therefore, NADESs offer endless opportunities for processes and can be applied in different research fields, mainly as solvents for the extraction or separation of contaminants, biocatalysis, leaching metals, science materials, and electrochemistry; in addition, they are sustainable and safe [12]. They have also been used to modify materials, such as polymers and silica, which are used in high-purity extraction and separation applications [13,14]. However, it is important to notice that other physical properties, such as polarity and viscosity, influence the results of the proposed technologies [15,16].

On the other hand, metal recycling is known to be the most developed area of the recycling field since, for most metals of commercial interest, major crises are expected due to the depletion of primary resources [17]. In the case of Zn–C batteries, the interest in their recycling has grown because it is estimated that more than 300,000 tons of Zn batteries are sold per year [18], and the most preferred route is hydrometallurgical.

In recent years, research has shifted towards the use of more environmentally friendly lixivants in the leaching of valuable metals [19]. Therefore, this work focuses on the leaching of metals such as zinc (Zn) and manganese (Mn) by using a NADES made from choline chloride and urea, proposing a new route for recycling spent batteries that could be more ecofriendly.

Multiple reports have demonstrated the ability of NADESs to digest common metal oxides [20–24], with certain compositions even rivaling the performance of acids [9]. Another advantage of using NADESs is that there is no need for an additional step involving a reducing agent and/or expensive solvent extractants, which are commonly added to many conventional hydrometallurgical procedures [25]. This process has recently been studied in the extraction separation of Ag (I) and Zn (II) from a synthetic nitrate leaching solution of spent silver oxide batteries via solvent extraction and stripping [26]. Furthermore, recently, green a choline chloride solvent was used for the recovery of copper from converter slag [27]. Others have proposed the use of these sustainable solvents as vehicles to enable the recycling of spent LIBs (rechargeable lithium-ion batteries) [28] with a DES of choline chloride or ethylene glycol (ChCl/EG).

The aim of this work is to propose an environmentally friendly Zn–C battery powder recycling process using a biodegradable NADES, for which a ChCl/urea dissolvent is used for the first time for the dissolution of Mn and Zn from these residues, studying the kinetics of the process as a function of temperature and solid/NADES ratio. For the preparation of the ChCl/urea, the proposed chemical reaction is based on a eutectic mixture commonly used as a deep eutectic solvent, mainly because the reagents used are relatively cheap, biodegradable, and do not require a high temperature for their preparation. Furthermore, choline chloride acts in the mixture as a compound with a hydrogen-accepting character (HBA), while urea donates hydrogen bonds, acting as an HBD, forming a compound commonly called reline [29,30]. Finally, the use of a NADES to perform the leaching step on the metal recovery of electronic scrap has attracted the attention of scientists as a new strategy to avoid the application of hazardous solvents and to achieve more sustainable processes since they are considered green solvents and are not environmentally toxic [24,31]. Moreover, they are easily prepared, which makes them cheaper than other alternative solvents, such as ionic liquids (ILs) [32].

2. Results and Discussion

2.1. Leaching Experiments

The dissolution of Zn and Mn oxides from spent zinc-carbon powder batteries using a NADES leaching agent can be explained in terms of the components of a NADES of ChCl, which have a significant influence on its physicochemical properties, such as polarity and dissolving capacity, which directly affect the extraction efficiency of metal compounds [33].

Overall, in all these procedures, extraction efficiency is dependent on many factors, such as the partition coefficient, type, and volume of the extracting and dispersive solvents; the sample volume; the analyte properties; the agitation; the ionic strength; the extraction time and temperature, etc. [34]. Figure 1 shows the leaching process at 25 °C as the function of time using a solid/NADES ratio of 3.3 g dm⁻³. As observed, after 4320 min (72 h), Zn oxides can be leached to almost ~90%, whereas Mn oxides reach ~30%. The high dissolution of Zn oxides, compared with the low dissolution of Mn oxides, can be explained by the difference in solubility, because, in general, zinc oxides are highly soluble, compared to those of manganese. Furthermore, it is well known that, of the Mn oxides, the Mn³⁺ and Mn⁴⁺ forms, which are present in zinc-carbon powder, are poorly soluble, and in fact, in acid solutions, they must first be reduced to Mn²⁺ [9,31,35]. On the other hand, neither Ni nor Mg was detected, while traces of Fe were observed. However, it is probable that the first two substances were found in small quantities, considering the initial composition of the powder (Table 1).

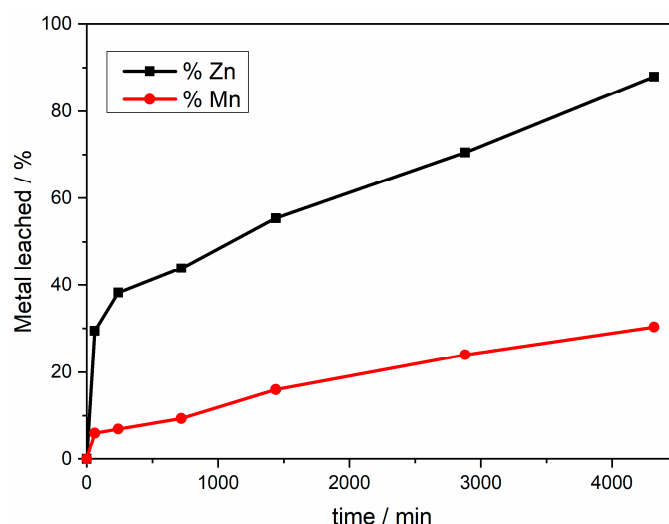


Figure 1. Metal leaching of spent zinc-carbon batteries.

Table 1. Chemical composition of the zinc-carbon battery powder.

Element	Content/wt %
Mn	48.83
Zn	13.02
Fe	1.12
Si	0.48
Ni	0.25
Mg	0.21
C	5.53
S	0.11

Figure 2 shows the Zn and Mn oxide leaching for both solid/NADES ratios of 3.3 and 10 g dm⁻³ for the four experimental temperatures: 80, 100, 125, and 150 °C. As observed, under the experimental conditions, it was possible to dissolve both Zn and Mn oxides in the NADES solution at a level greater than ~90% for both metals. Therefore, to explain the

observed behavior of the leaching experiments, modeling of the kinetics experiments has been carried out.

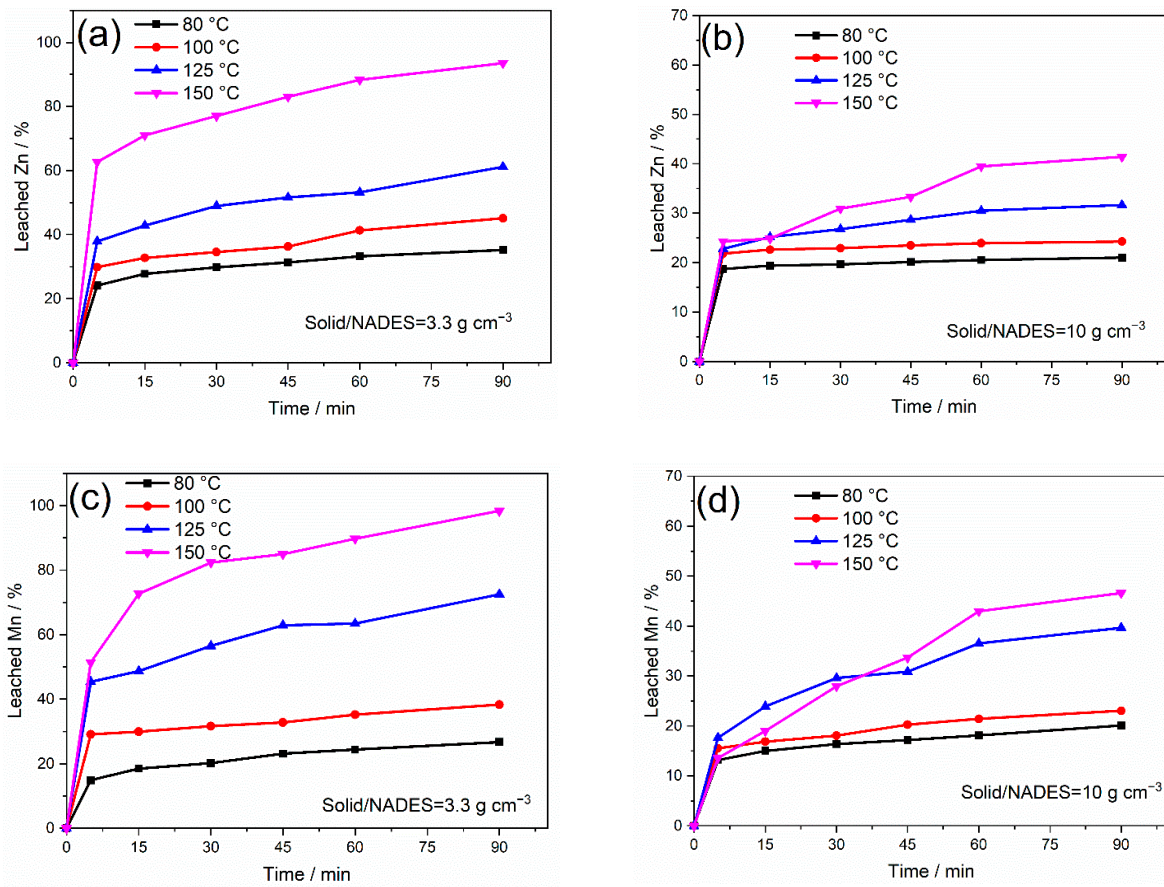


Figure 2. Zn and Mn oxide leaching for both solid/NADES ratios, as a function of temperature: (a) Zn oxides, 3.3 g dm⁻³; (b) Zn oxides, 10 g dm⁻³; (c) Mn oxides, 3.3 g dm⁻³; and (d) Mn oxides, 10 g dm⁻³.

Kinetic Modeling

For the kinetic modeling of the metal oxide leaching, spent zinc-carbon powder batteries were dissolved using a NADES as a leaching agent. Since the carbon would not react with the NADES, the Zn and Mn oxide dissolution proceeded in a topochemical manner, in which the inner core of the unreacted particle decreased with time [36].

Therefore, the leaching kinetics could be controlled by the diffusional mass transfer of either the NADES or the metal ions through a liquid boundary layer or a metal deposit [37]. If liquid film dissolution controls the reaction kinetics, the pseudo-first-order kinetic model (Equation (1)) or the second-order kinetic could be used (Equation (2)):

$$k_{app}t = -\ln(1 - x) \tag{1}$$

$$kt = \ln x^{-1} \tag{2}$$

where x is the fraction of the metal solubilized, t (min) is the reaction time, k_{app} (min⁻¹) is the pseudo-first-order kinetic constant, and k (min⁻¹) is the second-order constant. If product layer diffusion controls the kinetics, then the applied model should be a quadratic one, (Equation (3)), where k_d is the parabolic reaction constant (min⁻¹) [38]:

$$k_d t = x^2 \tag{3}$$

On the other hand, if the reaction kinetics is controlled by boundary layer, then the process can be evaluated in accordance with a shrinking sphere model (Equation (4)) [39] or the shrinking core model proposed by Ginstling–Brounstein (Equation (5)) [40]:

$$k_{ss}t = 1 - (1 - x)^{\frac{1}{3}} \tag{4}$$

$$k_{pl}t = 1 - \frac{2}{3}x - (1 - x)^{\frac{2}{3}} \tag{5}$$

where k_{ss} is the apparent rate constant of the shrinking sphere model (min^{-1}), whereas k_{pl} (min^{-1}) is the apparent rate constant of the shrinking core model with an insoluble product layer. For all cases, all of the k values were obtained for the four experimental temperatures, 80, 100, 125, and 150 °C (Figure 2) by applying least-squares regression analysis to both the solid/NADES ratios of 3.3 and 10 g dm^{-3} for Zn oxide leaching (see Table 2), and for Mn oxide leaching (see Table 3).

Table 2. Kinetic Parameters and fitting for Zn oxide leaching as a function of temperature. solid/NADES = 3.3 and 10 g dm^{-3} .

Kinetic Model		Solid/NADES = 3.3 g dm^{-3}				Solid/NADES = 10 g dm^{-3}			
		Temperature/°C							
		80	100	125	150	80	100	125	150
Pseudo-first-order	k_{app}/min^{-1}	1.75×10^{-3}	2.88×10^{-3}	5.18×10^{-3}	2.05×10^{-2}	3.23×10^{-4}	3.60×10^{-4}	1.42×10^{-3}	3.33×10^{-3}
	R^2	0.93	0.98	0.97	0.99	0.95	0.92	0.94	0.94
Second-order	k/min^{-1}	2.51×10^{-3}	4.66×10^{-3}	1.07×10^{-2}	1.47×10^{-1}	4.04×10^{-4}	4.69×10^{-4}	1.97×10^{-3}	5.02×10^{-3}
	R^2	0.95	0.97	0.97	0.93	0.95	0.92	0.94	0.93
Layer diffusion	k_d/min^{-1}	7.35×10^{-4}	1.34×10^{-3}	2.55×10^{-3}	5.61×10^{-3}	1.03×10^{-3}	1.28×10^{-4}	5.68×10^{-4}	1.46×10^{-3}
	R^2	0.95	0.97	0.97	0.96	0.96	0.92	0.95	0.94
Shrinking sphere model	k_{ss}/min^{-1}	5.17×10^{-4}	8.19×10^{-4}	1.36×10^{-3}	4.14×10^{-3}	1.00×10^{-4}	1.10×10^{-4}	7.64×10^{-4}	9.70×10^{-4}
	R^2	0.93	0.97	0.97	0.97	0.95	0.91	0.93	0.94
Shrinking core model	k_{pl}/min^{-1}	1.04×10^{-4}	2.05×10^{-4}	4.49×10^{-4}	1.78×10^{-3}	1.33×10^{-5}	1.69×10^{-5}	7.81×10^{-5}	2.13×10^{-4}
	R^2	0.96	0.98	0.99	0.99	0.97	0.95	0.96	0.96

Table 3. Kinetic Parameters and fitting for Mn oxide leaching as a function of temperature. solid/NADES = 3.3 and 10 g dm^{-3} .

Kinetic Model		Solid/NADES = 3.3 g dm^{-3}				Solid/NADES = 10 g dm^{-3}			
		Temperature/°C							
		80	100	125	150	80	100	125	150
Pseudo-first-order	k_{app}/min^{-1}	1.69×10^{-3}	1.66×10^{-3}	8.00×10^{-3}	3.59×10^{-2}	9.10×10^{-4}	1.12×10^{-3}	3.55×10^{-3}	5.97×10^{-3}
	R^2	0.94	0.99	0.97	0.93	0.96	0.97	0.93	0.95
Second-order	k/min^{-1}	2.15×10^{-3}	2.51×10^{-3}	2.09×10^{-2}	6.06×10^{-1}	1.10×10^{-3}	1.39×10^{-3}	5.10×10^{-3}	8.94×10^{-3}
	R^2	0.95	0.98	0.97	0.70	0.97	0.97	0.95	0.97
Layer diffusion	k_d/min^{-1}	5.65×10^{-4}	7.41×10^{-4}	3.75×10^{-3}	7.29×10^{-3}	2.55×10^{-4}	3.50×10^{-4}	1.47×10^{-3}	2.51×10^{-3}
	R^2	0.96	0.98	0.97	0.88	0.98	0.98	0.96	0.96
Shrinking sphere model	k_{ss}/min^{-1}	5.20×10^{-4}	4.83×10^{-4}	1.95×10^{-3}	5.60×10^{-3}	2.85×10^{-4}	3.47×10^{-4}	1.05×10^{-3}	1.75×10^{-3}
	R^2	0.93	0.98	0.97	0.95	0.96	0.97	0.93	0.95
Shrinking core model	k_{pl}/min^{-1}	7.38×10^{-5}	1.08×10^{-4}	7.53×10^{-4}	2.57×10^{-3}	3.20×10^{-5}	4.49×10^{-5}	2.08×10^{-4}	3.67×10^{-4}
	R^2	0.97	0.99	0.98	0.97	0.99	0.99	0.98	0.97

In general, experimental data obtained from the correlation presented a better fit with the shrinking core model, and the probable small deviation, especially for the Zn, could be related to the non-uniform size. Therefore, it can be stated that the resistance to diffusion through a product layer over the non-reacted particle surface controls the rate of reaction of the Zn–C batteries with NADES. This result is in good agreement with those observed in the literature for the leaching of spent batteries with H_2SO_4 [41], H_2SO_4 and ascorbic acid [42], and SO_2 [43].

From Figure 1, it is possible to establish the k_{pl} for Zn and Mn, also using Equation (5), at 25 °C. Thus, k_{pl} is equal to 3.56×10^{-5} ($R^2 = 0.97$) and $2.75 \times 10^{-6} \text{ min}^{-1}$ ($R^2 = 0.99$) for Zn and Mn, respectively.

2.2. Effect of Temperature and Solid/NADES Ratio

In order to clarify the leaching trend, Figure 3 shows the calculated k_{pl} as a function of the temperature and the solid/NADES ratio for both metals, and as expected, as the temperature rises, the leaching rate does as well. On the other hand, because the rate of a reaction is directly proportional to the value of k_{pl} , it is possible to observe the trend more clearly for Zn and Mn. As observed, until 100 °C is reached for all systems, the reaction rate is almost constant; however, as the temperature reaches 125 °C, the reaction rate rapidly increases, and therefore, it is a strongly temperature-activated process.

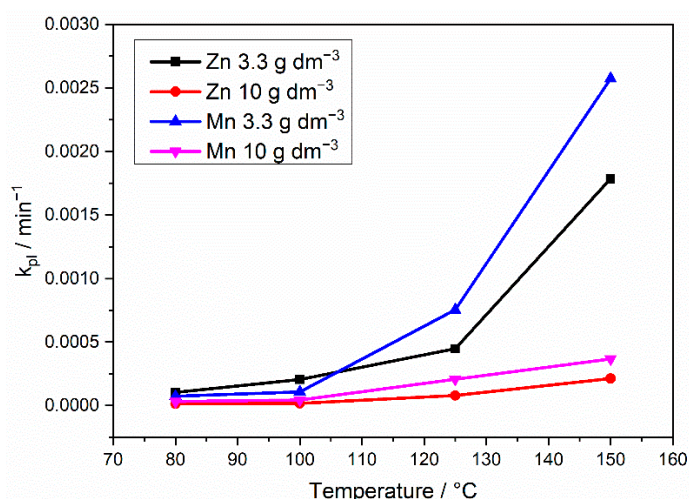


Figure 3. k_{pl} as function of temperature for the leaching of Zn and Mn oxides and solid/NADES ratio.

In addition, it can be observed that the reaction rate for the Mn oxides is higher than that observed for the Zn oxides. Furthermore, when the solid/NADES ratio increases, the reaction leaching rate decreases. Furthermore, this effect is strongly evident for both metals since the reaction rate at 150 °C increases 8 times for Zn (from $k_{pl} = 2.13 \times 10^{-4}$ to 1.78×10^{-3}) and 7 times (from $k_{pl} = 3.67 \times 10^{-4}$ to 2.57×10^{-3}) for Mn when the solid/NADES ratio decreases from 10 to 3.3 g dm⁻³. On the other hand, the decrease in the recovery for Zn and Mn that occurs as the solid/NADES ratio increases can be explained due to the solubility of metal oxides in NADES since it has been shown that the solubility increases due to the higher proton activity in DES compounds, and the dissolution is likely due to the formation of complexes with the urea or decomposition products of the urea, e.g., ammonia. Therefore, as the content of solid to be leached increases, there is a lower concentration of the decomposition products, and therefore, a lower dissolution [44].

2.3. Activation Energy

For reactions where the rate is high, it is possible to calculate the apparent activation energy through the Arrhenius equation:

$$\ln k_{pl} = -\frac{E_a}{RT} + \ln A \quad (6)$$

where k_{pl} is the rate constant shrinking core model, R is the ideal gas constant, T is the absolute temperature of the reaction, E_a is the apparent activation energy, and A is the pre-exponential factor. Therefore, the graph of the T^{-1} vs. $\ln k_{pl}$ allows the calculation of the activation energy (see Figure 4a,b) for Zn and Mn, respectively, for both solid/NADES ratio. The apparent activation energy value in the present investigation ranged from 49.13 to 52.21 kJ mol⁻¹ (11.74–12.47 kcal mol⁻¹) for Zn and from 46.97 to 66.77 kJ mol⁻¹ (11.25–15.96 kcal mol⁻¹) for Mn. It is important to mention that both values were higher than those reported for Mn and Zn dissolution from spent Zn–C batteries using inorganic acids: for Zn, it has been reported as 22.78 kJ mol⁻¹ [18], 23.03 [45], and 94.53 kJ mol⁻¹ [41], whereas for Mn, it has been reported as 7.04 [42], 31.80 [45], and 1.14 kJ mol⁻¹ [41].

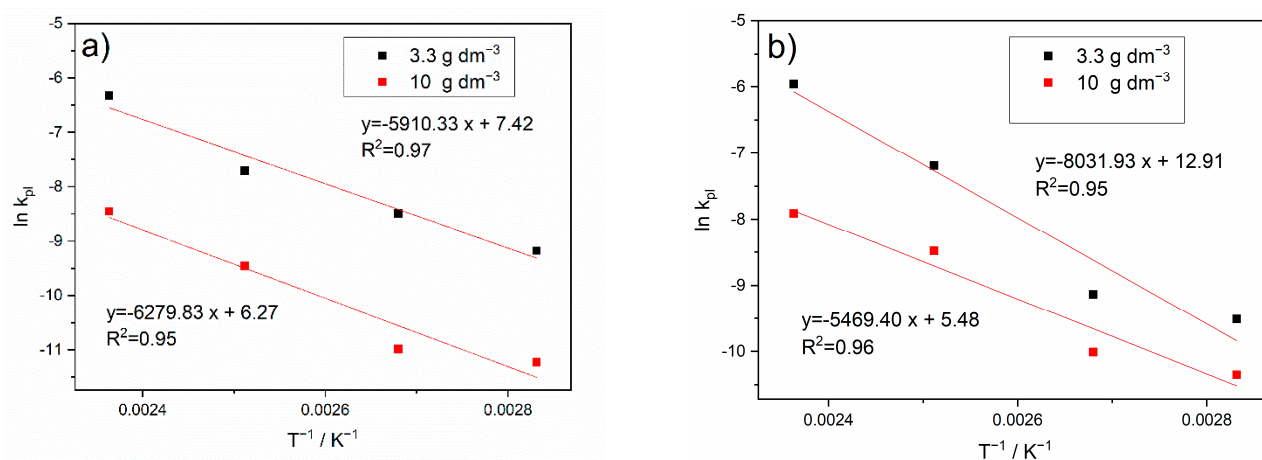


Figure 4. Arrhenius plots for (a) Zn and (b) Mn.

2.4. Final Solid Residue

Figure 5 presents the XRD diffraction pattern of the final solid residue after 90 min of leaching at 150 °C and a solid/NADES ratio of 3 g dm⁻³. As can be observed, the solid waste was composed mostly of graphite C (Graphite, ICSD 98-005-2230), and small remnants of ZnO (Zincite, ICSD 98-002-6170) and ZnMn₂O₄ (Hetaerolite, ICSD 98-001-5305). However, since the main goal of the leaching process is to achieve the maximum metallic dissolution of the waste, it is important to calculate the required time for maximum recovery. In the present study, using Equation (5), to leach the 99% of Zn at 80 °C, the required time should have been 2820 min, whereas for Mn, the calculated time should have been 3980 min. Since it is clear that the process is highly dependent on the temperature, the calculated times could be reduced to 165 and 125 min, for Zn and Mn, respectively, at 150 °C. However, it is preferable to keep the process temperature low due to environmental considerations, because, as the temperature increases, the formation of CO₂ and SO₂ due to the thermal effect is possible, which obviously must be avoided. However, it is evident that the main solid product to be obtained through the proposed process is made up of graphite, which can be reused in other processes.

Finally, regarding the solution leached with NADES, which contains Zn and Mn, it could be separated by electrodeposition processes. For example, it has been reported that it is possible to electrodeposit Zn contained in a NADES of choline chloride:ethylene glycol (ChCl:EG) on a steel substrate [46] or by using choline chloride (ChCl)/urea on copper [47]. Moreover, in the same medium, it has also been possible to electrodeposit Mn [45,48]. Therefore, it is a research topic to find the ideal separation conditions (additives, current, substrate, etc.) in order to obtain the optimal recovery. Furthermore, directly depositing both metals from the DES for the corrosion protection of Cu has also been proposed [49].

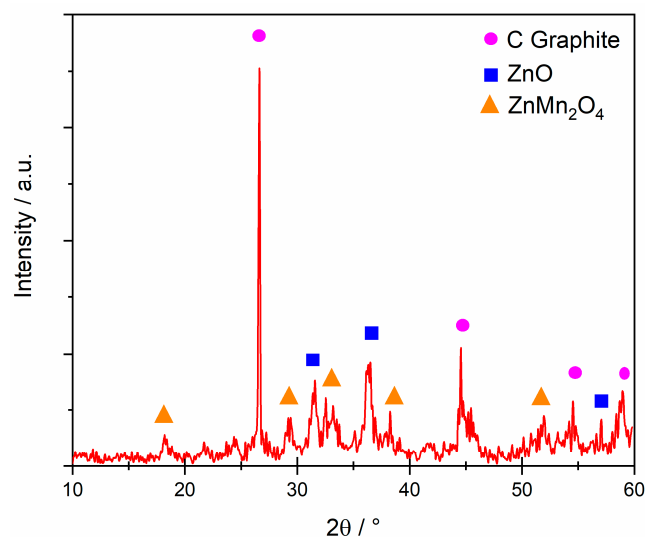


Figure 5. XRD pattern of solid residue after leaching: temperature 150 °C and solid/NADES ratio of 3 g dm⁻³.

3. Materials and Methods

3.1. ChCl/Urea NADES Preparation

For the preparation of the selected ChCl/urea NADES, choline chloride (ChCl, Sigma Aldrich ≥ 99%) (Saint Louis, MO, USA) and urea (Sigma Aldrich ≥ 97%) (Saint Louis, MO, USA) were used. The preparation of NADES was carried out with a molar ratio of ChCl-urea, 1:2, which is the most common composition, at a temperature of 85 °C and a stirring rate of 350 rpm in a glycerin water bath for approximately 2 h until a transparent product was obtained.

3.1.1. FTIR Studies

Figure 6 shows the FTIR spectra of urea, choline chloride, and NADES ChCl/urea (1:2 molar ratio). For pure urea, the 3432 and 3224 cm⁻¹ peaks correspond to N-H stretching vibrations, anti-symmetric and symmetric, respectively [50]. The peak at 1677 cm⁻¹ corresponds to the C=O, whereas the one at 1634 cm⁻¹ can be assigned to the deformation of N-H, and finally, the signal at 1457 cm⁻¹ corresponds to the stretching of the C-N group.

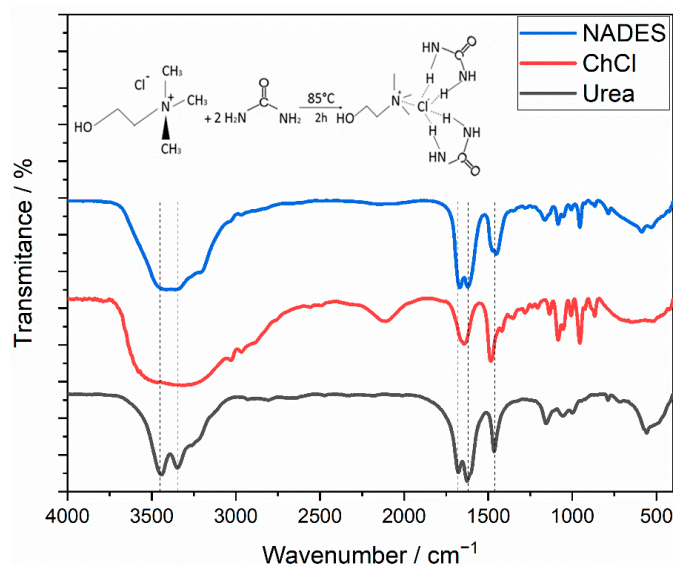


Figure 6. FTIR spectra of precursors: urea (bottom), choline chloride (middle), and synthesized NADES (urea/ChCl top).

For ChCl, characteristic bands can be observed at $3600\text{--}3200\text{ cm}^{-1}$, corresponding to O-H stretching. The vibrational bands at $2992\text{--}2851\text{ cm}^{-1}$ and 1485 cm^{-1} are correlated to an alkyl group; the 1485 cm^{-1} signal is particularly attributed to CH_2 bending, while the signal for the H-O bending can be observed at 1637 cm^{-1} . Finally, the band 869 cm^{-1} is assigned to C-C stretching [51].

The natural deep eutectic solvent (NADES) ChCl/urea shows, at $3396\text{--}3220\text{ cm}^{-1}$, stretching bands of the OH and N-H groups; the later appears as a large band deformed by hydrogen bond interactions of urea with choline. It is known that the NADES; urea/ChCl complex shows hydrogen bonds between the NH group of the urea and the Cl of the ChCl [52].

Moreover, the N-H and C=O stretching vibrations of the urea in NADES showed a slight blue shift, indicating the formation of hydrogen bonds between the amino group in the urea and the Cl of ChCl.

3.1.2. ^1H NMR Spectra

The chemical shifts were referenced to the quintuplet signal of residual methanol (CHD_2OD , δ 3.33). The chemical structure of each component was analyzed by ^1H NMR spectroscopy, which allows the identification of the different protons present in the molecules. In the ^1H NMR spectra shown in Figure 7, the characteristic signals of the NADES can be observed (Figure 7a ChCl + urea), urea (Figure 7b), and choline chloride (ChCl, Figure 7c).

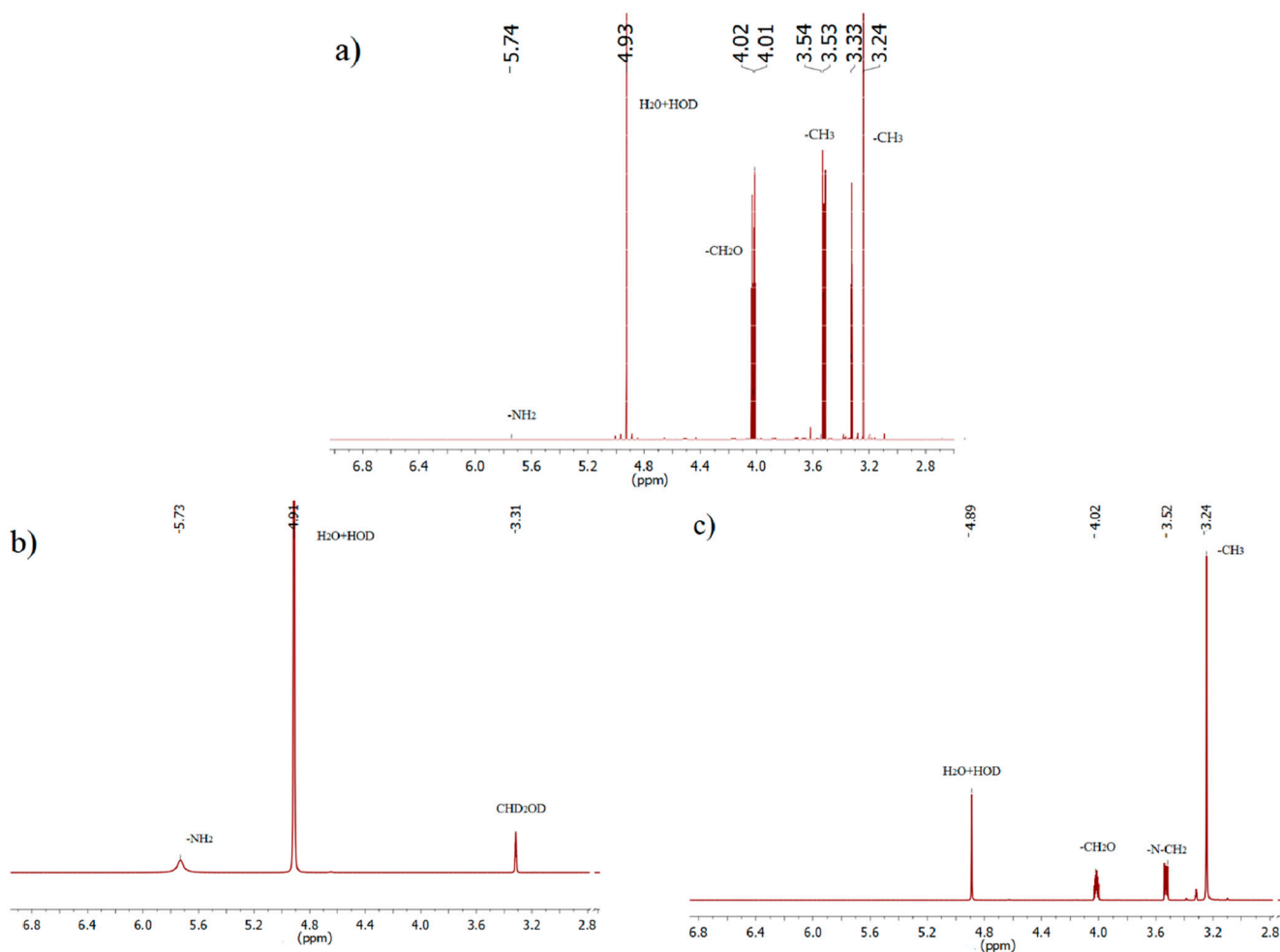


Figure 7. ^1H NMR spectra (500 MHz, methanol- d_4) of (a) NADES (choline chloride/urea), (b) urea, and (c) choline chloride.

In the NADES spectrum, the single signal at δ 3.24 belongs to the three-CH₃ groups. The multiplet signals at δ 3.52 can be attributed to the methylene protons attached to the N atom (N-CH₂), followed by the multiplet signals at δ 4.01 of the second methylene group (CH₂O). The broad signal at δ 5.73 belongs to the -NH₂ group of the urea.

The ¹H NMR spectrum of the urea only shows its typical broad signal at δ 5.73 of the NH₂ group. Finally, the ¹H NMR spectrum of choline chloride shows the singlet signals of the methyl groups (δ 3.23, 3 × CH₃), as well as those of the two methylene groups (δ 3.52, N-CH₂; δ 4.01, O-CH₂). It is worth mentioning that the signal of the OH group is not visible in the ChCl and ChCl + urea spectra due to the fact that this proton is exchangeable with the solvent (methanol-d₄). In the spectrum for choline chloride (ChCl, Figure 7c), the single signal at δ 4.89 corresponds to H₂O + OHD of impure deuterated methanol.

3.2. Zinc–Carbon Battery Powder

A mix of spent zinc-carbon batteries (types AA, D, and lantern) were collected from residual waste. The batteries were dismantled by first using a laboratory hammer crusher. Later, the steel cases, plastics, and papers were removed to obtain the typical black battery powder, which was later dried for 24 h at 100 °C. The dried battery powder was milled in a laboratory ball mill for 60 min. Subsequently, the obtained powder was sieved at $-88 \mu\text{m}$ (170 Tyler mesh). Figure 8a shows the scanning electron microscopy (SEM) image of the milled battery powder at a magnification of 250×; as observed, powders mainly present in an irregular form. The particle size distribution (see Figure 8b) was obtained by measuring 150 particles from several micrographs. The particle size ranged from 0.42 to 87.5 μm , (mean = 22.15 μm , median = 10 μm), and it was observed that the fine particles adhered to the larger ones.

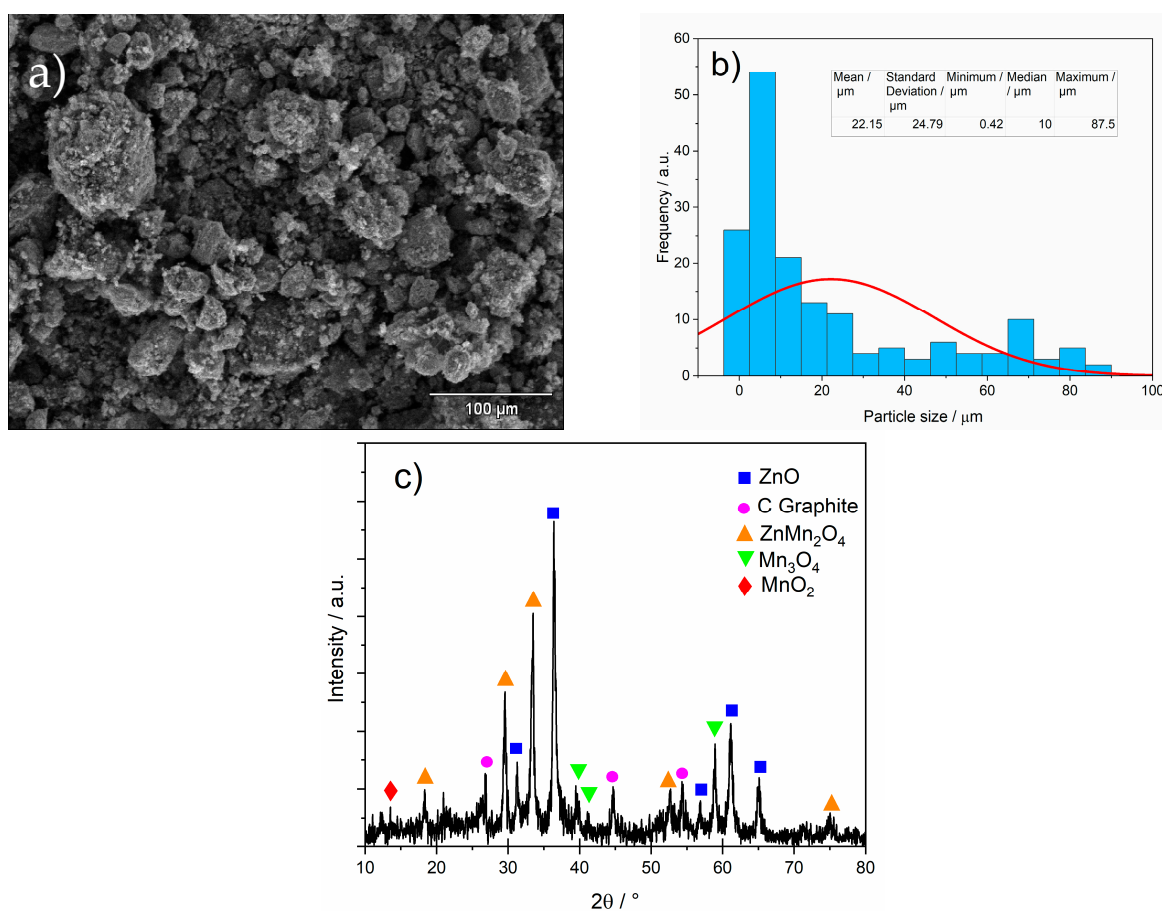


Figure 8. (a) Morphology of Zn–C battery powder by SEM: (b) particle size distribution, and (c) XRD pattern of the Zn–C battery powder.

Figure 8c presents the XRD pattern of the battery powder. It can be observed that the compounds were not completely crystalline; however, it was possible to identify that the powder was mainly composed of ZnO (Zincite, ICSD 98-002-6170), ZnMn_2O_4 (Hetaerolite, ICSD 98-001-5305), C (Graphite, ICSD 98-005-2230), Mn_3O_4 (Hausmannite, ICSD 98-003-0005), and MnO_2 (Manganasite, ICSD 98-002-0227). The present phases were similar to those reported by Majharul Haque Khan [53].

The chemical composition (Table 1) of the powder was determined by means of energy dispersive X-ray fluorescence (EDXRF) and was in good agreement with that found in the literature for Zn–C waste [54].

3.3. Leaching Experiments

Before the leaching experiments, the battery powder was carefully mixed to ensure homogeneity. The first leaching test was carried out at 25 °C, at 200 rpm for 4320 min (72 h) and with a solid/NADES ratio of 3.3 g dm⁻³. All the later leaching tests were carried out at isothermal conditions (80, 100, 125, and 150 °C) and stirred at 200 rpm. The choice of leaching temperatures was made with the criterion that they would present the widest range possible. The lower temperature (80 °C) was chosen because it was observed that the recovery of Zn and Mn is slow at 25 °C (Figure 1), in addition to the low recovery of Mn. On the other hand, the upper temperature (150 °C) was chosen because it is below the temperature at which NADES of $\text{CHCl}_3/\text{urea}$ has been reported to start to thermally decompose (≈ 170 °C) [55]. Additionally, two solid/NADES ratios were analyzed: 3.3 and 10 g dm⁻³. In this case, the choice was made based on preliminary experiments, in which it was observed that, at ratios greater than 10 g dm⁻³, the system did not present homogeneous agitation, in addition to the fact that, according to the results (see Figure 2), if the ratio increases, the recovery decreases. All of the leaching experiments were carried out in 90 min for comparative purposes since, at low temperatures, equilibrium is achieved in that time period (Figure 2).

3.4. Characterization

The initial composition of the Zn–C powder was determined by energy dispersive X-ray fluorescence (EDXRF) Rigaku NEX CG model. All zinc and manganese concentrations of the leaching solutions were determined by an atomic absorption spectrometer (AAS), Perkin Elmer Analyst 200 model. The NADES was studied by Fourier transform infrared and confocal micro-Raman spectroscopy (FTIR). NMR measurements were performed on a Varian (now Agilent) NMR System 500 spectrometer (Agilent Technologies, Inc., Santa Clara, CA, USA) operating at 500 MHz for ¹H NMR spectra. SEM observations were carried out in a JEOL 630, operating at 20 kV.

4. Conclusions

A natural deep eutectic liquid NADES was prepared from choline chloride and urea as a proposed medium for leaching and metal recovery processes with an environmentally friendly solvent. The system was tested to recycle Zn–C battery powders, with the aim of recovering Mn and Zn. The results showed that it is possible to leach 90% of Zn and 30% of Mn at room temperature in 72 h. The leaching time can be drastically decreased with an increase in temperature, achieving recovery of more than 90% for both metals at 150 °C. Regarding the kinetics, it was shown that the process can be modeled using the shrinking core model, so the resistance to diffusion through a product layer over the non-reacted particle surface controls the rate of reaction of the Zn–C batteries with the NADES.

Author Contributions: I.G.C.-R.: methodology and investigation; J.A.M.-P.: investigation and validation; R.R.-G.: visualization, investigation, reviewing, and editing; D.Y.M.-V.: investigation and validation. L.G.Z.-V.: investigation; Á.d.J.M.-R.: conceptualization, supervision, writing—reviewing and editing. All authors have read and agreed to the published version of the manuscript.

Funding: This work was supported by the Instituto Politécnico Nacional (SIP project 20221369).

Institutional Review Board Statement: Not applicable.

Informed Consent Statement: Not applicable.

Data Availability Statement: Not applicable.

Acknowledgments: The Consejo Nacional de Ciencia y Tecnología, CONACyT and the Laboratories of Chemical Analysis of the IPN. The authors wish to make a posthumous tribute to the memory of María del Rosario Ruiz Guerrero, collaborator and friend.

Conflicts of Interest: The authors declare no conflict of interest.

References

1. Zhu, S.; Zhou, J.; Jia, H.; Zhang, H. Liquid–liquid microextraction of synthetic pigments in beverages using a hydrophobic deep eutectic solvent. *Food Chem.* **2018**, *243*, 351–356. [[CrossRef](#)] [[PubMed](#)]
2. Zhang, Q.; De Oliveira Vigier, K.; Royer, S.; Jérôme, F. Deep eutectic solvents: Syntheses, properties and applications. *Chem. Soc. Rev.* **2012**, *41*, 7108–7146. [[CrossRef](#)] [[PubMed](#)]
3. Abbott, A.P.; Capper, G.; Davies, D.L.; Rasheed, R.K.; Tambyrajah, V. Novel solvent properties of choline chloride/urea mixtures. *Chem. Commun.* **2003**, *39*, 70–71. [[CrossRef](#)] [[PubMed](#)]
4. Tomé, L.I.N.; Baião, V.; da Silva, W.; Brett, C.M.A. Deep eutectic solvents for the production and application of new materials. *Appl. Mater. Today* **2018**, *10*, 30–50. [[CrossRef](#)]
5. Stefanovic, R.; Ludwig, M.; Webber, G.B.; Atkin, R.; Page, A.J. Nanostructure, hydrogen bonding and rheology in choline chloride deep eutectic solvents as a function of the hydrogen bond donor. *Phys. Chem. Chem. Phys.* **2016**, *19*, 3297–3306. [[CrossRef](#)]
6. Zhekenov, T.; Toksanbayev, N.; Kazakbayeva, Z.; Shah, D.; Mjalli, F.S. Formation of type III Deep Eutectic Solvents and effect of water on their intermolecular interactions. *Fluid Phase Equilibria* **2017**, *441*, 43–48. [[CrossRef](#)]
7. Singh, M.B.; Kumar, V.S.; Chaudhary, M.; Singh, P. A mini review on synthesis, properties and applications of deep eutectic solvents. *J. Indian Chem. Soc.* **2021**, *98*, 100210. [[CrossRef](#)]
8. Abbott, A.P.; Boothby, D.; Capper, G.; Davies, D.L.; Rasheed, R.K. Deep Eutectic Solvents Formed between Choline Chloride and Carboxylic Acids: Versatile Alternatives to Ionic Liquids. *J. Am. Chem. Soc.* **2004**, *126*, 9142–9147. [[CrossRef](#)]
9. Abbott, A.P.; Capper, G.; Davies, D.L.; McKenzie, K.J.; Obi, S.U. Solubility of Metal Oxides in Deep Eutectic Solvents Based on Choline Chloride. *J. Chem. Eng. Data* **2006**, *51*, 1280–1282. [[CrossRef](#)]
10. Durand, E.; Lecomte, J.; Baréa, B.; Villeneuve, P. Towards a better understanding of how to improve lipase-catalyzed reactions using deep eutectic solvents based on choline chloride. *Eur. J. Lipid Sci. Technol.* **2013**, *116*, 16–23. [[CrossRef](#)]
11. Panić, M.; Andlar, M.; Tišma, M.; Rezić, T.; Šibalić, D.; Bubalo, M.C.; Redovniković, I.R. Natural deep eutectic solvent as a unique solvent for valorisation of orange peel waste by the integrated biorefinery approach. *Waste Manag.* **2020**, *120*, 340–350. [[CrossRef](#)] [[PubMed](#)]
12. Martins, M.; Aroso, I.M.; Reis, R.L.; Duarte, A.R.C.; Craveiro, R.; Paiva, A. Enhanced performance of supercritical fluid foaming of natural-based polymers by deep eutectic solvent. *AIChE J.* **2014**, *60*, 3701–3706. [[CrossRef](#)]
13. Anastas, P.T.; Williamson, T.C. *Green Chemistry: An Overview*; Chapter 1; ACS American Chemical Society: Washington, DC, USA, 1996; pp. 1–17.
14. Anastas, P.T.; Warner, J.C. *Green Chemistry: Theory and Practice*; Oxford University Press: New York, NY, USA, 1998.
15. Francisco, M.; van der Bruinhorst, A.; Kroon, M.C. Low-Transition-Temperature Mixtures (LTTMs): A New Generation of Designer Solvents. *Angew. Chem. Int. Ed.* **2013**, *52*, 3074–3085. [[CrossRef](#)] [[PubMed](#)]
16. Wei, Z.; Qi, X.; Li, T.; Luo, M.; Wang, W.; Zu, Y.; Fu, Y. Application of natural deep eutectic solvents for extraction and determination of phenolics in *Cajanus cajan* leaves by ultra performance liquid chromatography. *Sep. Purif. Technol.* **2015**, *149*, 237–244. [[CrossRef](#)]
17. Buzatu, M.; Săceanu, S.; Petrescu, M.; Ghica, G.; Buzatu, T. Recovery of zinc and manganese from spent batteries by reductive leaching in acidic media. *J. Power Sources* **2014**, *247*, 612–617. [[CrossRef](#)]
18. Baba, A.; Adekola, A.; Bale, R. Development of a combined pyro- and hydro-metallurgical route to treat spent zinc–carbon batteries. *J. Hazard. Mater.* **2009**, *171*, 838–844. [[CrossRef](#)]
19. Musariri, B.; Akdogan, G.; Dorfling, C.; Bradshaw, S. Evaluating organic acids as alternative leaching reagents for metal recovery from lithium ion batteries. *Miner. Eng.* **2019**, *137*, 108–117. [[CrossRef](#)]
20. Albler, F.J.; Bica, K.; Foreman, M.R.S.J.; Holgersson, S.; Tyumentsev, J. A comparison of two methods of recovering cobalt from a deep eutectic solvent: Implications for battery recycling. *Clean. Prod.* **2017**, *167*, 806–814. [[CrossRef](#)]
21. Foreman, M.R. Progress towards a process for the recycling of nickel metal hydride electric cells using a deep eutectic solvent. *Cogent Chem.* **2016**, *2*, 1139289. [[CrossRef](#)]
22. Millia, L.; Dall’Asta, V.; Ferrara, C.; Berbenni, V.; Quartarone, E.; Perna, F.M.; Capriati, V.; Mustarelli, P. Bio-inspired choline chloride-based deep eutectic solvents as electrolytes for lithium-ion batteries. *Solid State Ionics* **2018**, *323*, 44–48. [[CrossRef](#)]
23. Tang, B.; Zhang, H.; Row, K.H. Application of deep eutectic solvents in the extraction and separation of target compounds from various samples. *J. Sep. Sci.* **2015**, *38*, 1053–1064. [[CrossRef](#)]

24. Smith, E.L.; Abbott, A.P.; Ryder, K.S. Deep Eutectic Solvents (DESs) and Their Applications. *Chem. Rev.* **2014**, *114*, 11060–11082. [[CrossRef](#)]
25. Yao, Y.; Zhu, M.; Zhao, Z.; Tong, B.; Fan, Y.; Hua, Z. Hydrometallurgical processes for recycling spent Lithium-Ion batteries: A critical review, ACS Sustain. *Chem. Eng.* **2018**, *6*, 13611–13627. [[CrossRef](#)]
26. Sung-Yong, C.; Won-Geun, L.; Pan-Pan, S. Solvent Extraction Separation of Silver(I) and Zinc(II) from Nitrate Leach Solution of Spent Silver Oxide Batteries with D2EHPA. *Mat. Trans.* **2019**, *60*, 1090–1095. [[CrossRef](#)]
27. Topçu, M.; Rüsen, A.; Küçük, Ö. Treatment of copper converter slag with deep eutectic solvent as green chemical. *Waste Manag.* **2021**, *132*, 64–73. [[CrossRef](#)]
28. Tran, M.K.; Rodrigues, M.-T.F.F.; Kato, K.; Babu, G.; Ajayan, P.M. Deep eutectic solvents for cathode recycling of Li-ion batteries. *Nat. Energy* **2019**, *4*, 339–345. [[CrossRef](#)]
29. Alonso, D.A.; Baeza, A.; Chinchilla, R.; Gomez, C.; Guillen, G.; Maset, X.; Pastor, I.M.; Ramon, D.J.; Níguez, D.R.; Saavedra, B. Eutectic mixtures as a sustainable alternative to solvents conventions in Organic Chemistry. *An. Quím.* **2018**, *114*, 79–87.
30. Hammond, O.S.; Bowron, D.T.; Edler, K.J. Liquid structure of the choline chloride-urea deep eutectic solvent (reline) from neutron diffraction and atomistic modelling. *Green Chem.* **2016**, *18*, 2736–2744. [[CrossRef](#)]
31. Li, G.; Deng, D.; Chen, Y.; Shan, Y.; Ai, N. Solubilities and thermodynamic properties of CO₂ in choline-chloride based deep eutectic solvents. *J. Chem. Thermodyn.* **2014**, *75*, 58–62. [[CrossRef](#)]
32. Dias, R.M.; da Costa, M.C.; Jimenez, Y.P. Perspectives of Using DES-Based Systems for Solid–Liquid and Liquid–Liquid Extraction of Metals from E-Waste. *Minerals* **2022**, *12*, 710. [[CrossRef](#)]
33. Liu, W.; Zhang, K.; Chen, J.; Yu, J. Ascorbic acid and choline chloride: A new natural deep eutectic solvent for extracting ter-butylhydroquinone antioxidant. *J. Molec. Liq.* **2018**, *260*, 173–179. [[CrossRef](#)]
34. Cunha, S.C.; Fernandes, J.O.; Oliveira, M.B.P.P. *Strategies for Pesticides Analysis*, 1st ed.; InTech: Rijeka, Croatia, 2011.
35. Chen, W.-S.; Liao, C.-T.; Lin, K.-Y. Recovery Zinc and Manganese from Spent Battery Powder by Hydrometallurgical Route. *Energy Procedia* **2017**, *107*, 167–174. [[CrossRef](#)]
36. Abdel-Aal, E.; Rashad, M. Kinetic study on the leaching of spent nickel oxide catalyst with sulfuric acid. *Hydrometallurgy* **2004**, *74*, 189–194. [[CrossRef](#)]
37. Mishra, D.; Kim, D.J.; Ralph, D.E.; Ahn, J.G.; Rhee, Y.H. Bioleaching of spent hydro-processing catalyst using acidophilic bacteria and its kinetics aspect. *J. Hazard. Mater.* **2008**, *152*, 1082–1091. [[CrossRef](#)]
38. Dickinson, C.; Heal, G. Solid–liquid diffusioncontrolled rate equations. *Thermochim. Acta* **1999**, *340–341*, 89–103. [[CrossRef](#)]
39. Senanayake, G. A mixed surface reaction kinetic model for the reductive leaching of manganese dioxide with acidic sulfur dioxide. *Hydrometallurgy* **2004**, *73*, 215–224. [[CrossRef](#)]
40. Senanayake, G.; Das, G. A comparative study of leaching kinetics of limonitic laterite and synthetic iron oxides in sulfuric acid containing sulfur dioxide. *Hydrometallurgy* **2004**, *72*, 59–72. [[CrossRef](#)]
41. Agacayak, T.; Aras, A. Investigation of Dissolution Kinetics of Zinc and Manganese From Spent Zinc-Carbon Batteries in Sulphuric Acid Solution. *Turk. J. Eng.* **2018**, *2*, 107–112. [[CrossRef](#)]
42. Kursunoglu, S.; Kaya, M. Dissolution and precipitation of zinc and manganese obtained from spent zinc-carbon and alkaline battery powder. *Physicochem. Probl. Miner. Process.* **2014**, *50*, 41–45. [[CrossRef](#)]
43. Avraamides, J.; Senanayake, G.; Clegg, R. Sulfur dioxide leaching of spent Zinc-Carbon battery scrap. *J. Power Sources* **2006**, *159*, 1488–1493. [[CrossRef](#)]
44. Pateli, I.M.; Thompson, D.; Alabdullah, S.S.M.; Abbott, A.P.; Jenkin, G.R.T.; Hartley, J.M. The effect of pH and hydrogen bond donor on the dissolution of metal oxides in deep eutectic solvents. *Green Chem.* **2020**, *22*, 5476–5486. [[CrossRef](#)]
45. Taner, H.A.; Aras, A.; Agacayak, T. Leaching of zinc- carbon batteries in acetic acid solution. *Int. Acad. Res. Congr.* **2016**, *4*, 231–236. [[CrossRef](#)]
46. Pereira, N.M.; Pereira, C.M.; Araújo, J.P.; Silva, A.F. Zinc Electrodeposition from deep eutectic solvent containing organic additives. *J. Electroanal. Chem.* **2017**, *801*, 545–551. [[CrossRef](#)]
47. Xie, X.; Zou, X.; Lu, X.; Lu, C.; Cheng, H.; Xu, Q.; Zhou, Z. Electrodeposition of Zn and Cu–Zn alloy from ZnO/CuO precursors in deep eutectic solvent. *Appl. Surf. Sci.* **2016**, *385*, 481–489. [[CrossRef](#)]
48. Pereira, N.M.; Pereira, C.M.; Araújo, J.P.; Silva, A.F. Electrodeposition of Mn and Mn-Sn Alloy Using Choline Chloride-Based Ionic Liquids. *J. Electrochem. Soc.* **2017**, *164*, D486–D492. [[CrossRef](#)]
49. Fashu, S.; Gu, C.D.; Zhang, J.L.; Zheng, H.; Wang, X.L.; Tu, J.P. Electrodeposition, Morphology, Composition, and Corrosion Performance of Zn-Mn Coatings from a Deep Eutectic Solvent. *J. Mater. Eng. Perform.* **2014**, *24*, 434–444. [[CrossRef](#)]
50. Yue, D.; Jia, Y.; Yao, Y.; Sun, J.; Jing, Y. Structure and electrochemical behavior of ionic liquid analogue based on choline chloride and urea. *Electrochim. Acta* **2012**, *65*, 30–36. [[CrossRef](#)]
51. Deng, L.; Jing, Y.; Sun, J.; Ma, J.; Yue, D.; Wang, H. Preparation and properties of a moisture-stable ionic liquid ChCl–ZnCl₂–MgCl₂·2CH₃COOCH₂CH₃·2H₂O. *J. Mol. Liq.* **2012**, *170*, 45–50. [[CrossRef](#)]
52. Song, X.; Hu, W.; Huang, W.; Wang, H.; Yan, S.; Yu, S.; Liu, F. Methanolysis of polycarbonate into valuable product bisphenol A using choline chloride-based deep eutectic solvents as highly active catalysts. *Chem. Eng. J.* **2020**, *388*, 124324. [[CrossRef](#)]
53. Khan, M.H.; Kurny, A. Characterization of Spent Household Zinc-Carbon Dry Cell Batteries in the Process of Recovery of Value Metals. *J. Miner. Mater. Charact. Eng.* **2012**, *11*, 641–651. [[CrossRef](#)]

-
54. Sadeghi, S.M.; Jesus, J.; Soares, H.M. A critical updated review of the hydrometallurgical routes for recycling zinc and manganese from spent zinc-based batteries. *Waste Manag.* **2020**, *113*, 342–350. [[CrossRef](#)] [[PubMed](#)]
 55. Delgado-Mellado, N.; Larriba, M.; Navarro, P.; Rigual, V.; Ayuso, M.; García, J.; Rodríguez, F. Thermal stability of choline chloride deep eutectic solvents by TGA/FTIR-ATR analysis. *J. Mol. Liq.* **2018**, *260*, 37–43. [[CrossRef](#)]